Domain Features of the Peripheral Stalk Subunit H of the Methanogenic A_1A_O ATP Synthase and the NMR Solution Structure of $H_{1\text{-}47}$

Goran Biuković, Shovanlal Gayen, Konstantin Pervushin, and Gerhard Grüber*
School of Biological Sciences, Nanyang Technological University, Singapore

ABSTRACT A series of truncated forms of subunit H were generated to establish the domain features of that protein. Circular dichroism analysis demonstrated that H is divided at least into a C-terminal coiled-coil domain within residues 54–104, and an N-terminal domain formed by adjacent α-helices. With a cysteine at the C-terminus of each of the truncated proteins ($H_{1\text{-}47}$, $H_{1\text{-}54}$, $H_{1\text{-}59}$, $H_{1\text{-}61}$, $H_{1\text{-}67}$, $H_{1\text{-}69}$, $H_{1\text{-}71}$, $H_{1\text{-}78}$, $H_{1\text{-}80}$, $H_{1\text{-}91}$, and $H_{47\text{-}105}$), the residues involved in formation of the coiled-coil interface were determined. Proteins $H_{1\text{-}54}$, $H_{1\text{-}61}$, $H_{1\text{-}69}$, and $H_{1\text{-}80}$ showed strong cross-link formation, which was weaker in $H_{1\text{-}47}$, $H_{1\text{-}59}$, $H_{1\text{-}71}$, and $H_{1\text{-}91}$. A shift in disulfide formation between cysteins at positions 71 and 80 reflected an interruption in the periodicity of hydrophobic residues in the region $_{71}$AEKILEETEKE$_{81}$. To understand how the N-terminal domain of H is formed, we determined for the first time, to our knowledge, the solution NMR structure of $H_{1\text{-}47}$, which revealed an α-helix between residues 15–42 and a flexible N-terminal stretch. The α-helix includes a kink that would bring the two helices of the C-terminus into the coiled-coil arrangement. $H_{1\text{-}47}$ revealed a strip of alanines involved in dimerization, which were tested by exchange to single cysteines in subunit H mutants.

INTRODUCTION

The A_1A_O ATP synthase (A-ATP synthase) catalyzes the process of ATP synthesis from ADP and inorganic phosphate in archaea. The membrane-integrated enzyme comprises the subunits A–H, *a*, and *c* in the stoichiometry of A_3:B_3:C:D:E_2:F:G:H_2:*a*:c_x (1–3). This complex is composed of the A_1 headpiece, A_3:B_3, which is attached by a central stalk and two peripheral stalks to a membrane-embedded ion-translocating part known as A_O, and a collar-like structure (4,5) that is composed of subunit E (6). The central stalk is made of subunits C, D, and F (7,8), whereas the peripheral stalks are formed by the subunit H and the N-terminal domain of subunit *a*, respectively (9). ATP is synthesized or hydrolyzed on the A_3:B_3 headpiece, and the energy provided for or released during that process is transmitted to the membrane-bound A_O domain, which consists of subunits *a* and *c*. The energy coupling between the two active domains occurs via the stalk part(s) (7–9).

Since 2006, high-resolution crystal structures have been available for the nucleotide-binding subunits A (10) and B (11) of the A-ATP synthase, providing information on the nucleotide-binding sites. Significant insights into the central stalk and collar-domain came from the high-resolution structure of subunits C (12,13) and F (14), and the C-terminal domain of subunit E (15), respectively, and also from the crystallographic structure of the *c*-ring of the A_O domain (16). Recently, the low-resolution structure of subunit H was determined from SAXS data (17). Subunit H is dimeric in solution and has a boomerang-like shape that is divided into two arms 120 Å and 60 Å in length (17). CD spectroscopy revealed that 80% of H is α-helical, and the rest is in a coiled-coil arrangement (17). Studies using NMR and intrinsic fluorescence spectroscopy have identified the N-terminal (residues 1–24) and C-terminal (residues 98–104) regions of subunit H as associating with the N-terminal domains of subunit E (6) and A (17), respectively. Therefore, the H subunit provides a critical link between the so-called collar-like domain and the catalytic A subunit.

In this study, we first focused on determining the region(s) that form the coiled-coil domain and thereby the dimerization segment of subunit H. We analyzed several constructs of subunit H truncated at the N- or C-terminus by CD spectroscopy, which demonstrated the role of the C-terminal region in the coiled-coil arrangement. A cysteine residue introduced at the very C-terminus of each of the 11 constructs resulted in a different intersubunit disulfide pattern, providing insight into the proximity of the residues. Finally, the solution structure of the N-terminal segment $H_{1\text{-}47}$, which is involved in subunit H and E assembly (6), was determined by NMR spectroscopy. (The coordinates for the structure of $H_{1\text{-}47}$ have been deposited in the Protein Data Bank with code 2k6i.)

Submitted September 24, 2008, and accepted for publication April 16, 2009.

Goran Biuković and Shovanlal Gayen contributed equally to this work.

*Correspondence: ggrueber@ntu.edu.sg

Abbreviations: CD, circular dichroism; DSS, 2, 2-dimethyl-2-silapentane-5-sulphonate; DTT, dithiothreitol; EDTA, ethylenediaminetetraacetic acid; HSQC, heteronuclear single quantum coherence; IPTG, isopropyl-β-D-thio-galactoside; NMR, nuclear magnetic resonance; NOE, nuclear Overhauser effect; NOESY, NOE spectroscopy; NTA, nitrilotriacetic acid; PAGE, polyacrylamide gel electrophoresis; PCR, polymerase chain reaction; PFG, pulsed field gradient; SAXS, small-angle x-ray scattering; R_1, longitudinal relaxation time; R_2, transverse relaxation time; RMSD, root mean-square deviation; SDS, sodium dodecyl sulfate; TOCSY, total correlation spectroscopy; Tris, Tris-(hydroxymethyl)aminomethane.

Editor: Marc Baldus.

0006-3495/09/07/0286/9 $2.00

doi: 10.1016/j.bpj.2009.04.026

MATERIALS AND METHODS

Biochemicals

Pfu DNA polymerase and Ni^{2+}-NTA-chromatography resin were obtained from QIAGEN (Hilden, Germany), and restriction enzymes were purchased from MBI Fermentas (St. Leon-Rot, Germany). Chemicals for gel electrophoresis and trypsin used for in-gel digestion were purchased from Serva (Heidelberg, Germany) and Promega (Madison, WI), respectively. All other chemicals were of analytical grade and obtained from BIOMOL (Hamburg, Germany), Merck (Darmstadt, Germany), Sigma (Deisenhofen, Germany), or Serva (Heidelberg, Germany). $(^{15}NH_4)_2SO_4$ and (^{13}C) glucose were purchased from Cambridge Isotope Laboratories (Andover, MA).

Cloning, expression, and protein purification

To obtain the truncated H subunits, including the residues H_{1-54}, H_{1-59}, H_{1-61}, H_{1-67}, H_{1-69}, H_{1-71}, H_{1-78}, H_{1-80}, H_{1-91}, and H_{47-105}, respectively, the following primers were designed: forward primer 5′-GGA ACC ATG GGC GTT AGT GTT ATG-3′, and accordingly the reverse primers: 5′-TCT GAG CTC CTC AAC ACT TTG CC-3′ (H_{1-54}), 5′-TCG GAG CTC TTA ACA CTC TTC AAC AA-3′ (H_{1-59}), 5′-CTT CTT CGA GCT CTT AAC AAA TCA TCT CTT CA-3′ (H_{1-61}), 5′-CAG CGA GCT CTC AGC ATT CTT C-3′ (H_{1-67}), 5′-AAT CTT TGA GCT CTT AAC ACT TTG CTT CTT C-3′ (H_{1-69}), 5′-CTT CGA GCT CCT TTC AGC ATT CTT-3′ (H_{1-71}), 5′-CAG GAG CTC TTA ACA CTC TTC AAG AAT C-3′ (H_{1-78}), 5′-GAT TTC TTT GAG CTC TTA GCA TTC TGT CTC TTC-3′ (H_{1-80}), 5′-CGA GAG CTC CTA ACA CTT GGC AAT G-3′ (H_{1-91}). To generate the recombinant protein H_{47-105}, the forward primer 5′-AAA CTC ACC ATG GAA GCT GAA GA-3′ and the reverse primer 5′-CAC CTG AGC TCT TAA CAA ATC TCA A-3′ were used. Each of the 11 constructs has a cysteine residue introduced at the very C-terminus, which enabled us to study possible Cys-Cys interactions. The genomic DNA from *Methanocaldococcus jannaschii* ATCC No. 43067D was used as the template. The pET9d-His_3 vector (18) containing the respective gene was transformed into *Escherichia coli* cells (strain BL21 (DE3)). To induce production of the recombinant proteins, the cultures were supplemented with IPTG to a final concentration of 1 mM. The harvested cells were lysed on ice in buffer A (50 mM Tris/HCl, pH 7.5, 250 mM NaCl, and 4 mM Pefabloc SC (BIOMOL)). The lysate was incubated in a waterbath for 20 min at 65°C and precipitated material was separated by centrifugation at 10,000 $\times$ *g* for 35 min. The supernatant was filtered (0.45 μm; Millipore, Singapore) and passed over a 3 mL Ni^{2+}-NTA resin column to isolate H_{1-54}, H_{1-59}, H_{1-61}, H_{1-67}, H_{1-69}, H_{1-71}, H_{1-78}, H_{1-80}, H_{1-91} and H_{47-105}, respectively, according to Biuković et al. (17). The His-tagged protein was allowed to bind to the matrix for 1.5 h at 4°C and eluted with an imidazole-gradient (25–250 mM) in buffer A. Fractions containing His_3-H_{1-54}, H_{1-59}, H_{1-61}, H_{1-67}, H_{1-69}, H_{1-71}, H_{1-78}, H_{1-80}, H_{1-91}, and H_{47-105}, respectively, were identified by SDS-PAGE (19), pooled and subsequently applied on an ion-exchange column (Resource Q, 6 mL; GE Healthcare). The protein was eluted by a linear NaCl gradient (50 mM to 1 M). The proteins were concentrated using Centricon YM-3 (3 kDa molecular mass cutoff) spin concentrators (Millipore). The N-terminal protein H_{1-47} was generated and isolated as described previously (17). The purity of all protein samples was analyzed by SDS-PAGE (19). SDS-polyacrylamide gels were stained with Coomassie Brilliant Blue G250. Protein concentrations were determined by the bicinchoninic acid assay (BCA; Pierce, Rockford, IL).

The subunit H mutants A19C, A26C, A35C, and A37C were generated by the overlap extension PCR method (20) using gene *atpH* as a template (17). In two PCR reactions one flanking primer 5′-GGA ACC ATG GGC GTT AGT GTT ATG-3′ (forward primer) and 5′-AATCACCTGAGCTCTTA AATCTCAAGAATC-3′ (reverse primer), which anneal at both ends of the gene *atpH*, were used. The following internal primers were used to generate the five different subunit H mutants: A19C internal forward 5′-A GCT GAA GAA CAG TGC GTT AAA GAA ATA GA-3′; A19C internal reverse: 5′-CTC TAT TTC TTT AAC GCA CTG TTC TTC AGC-3′; A26C internal forward: 5′-GAA ATA GAG GAA TGC AAG AAT AGA GCT GAG -3′; A26C internal reverse: 5′-CTC AGC TCT ATT CTT GCA TTC CTC TAT TTC -3′; A35C internal forward: 5′-CTG AGC AGA TAA AGT GCG AGG CAA T-3′; A35C internal reverse: 5′- ATT GCC TCG CAC TTT ATC TGC TCA G-3′; A37C internal forward: 5′-CAG ATA AAG GCA GAG TGT ATT GAA GAA GCA-3′; and A37C internal reverse: 5′-TGC TTC TTC AAT ACA CTC TGC CTT TAT CTG-3′. After digestion with *Nco*I and *Sac*I, the PCR product was ligated into the pET9d-His_3 vector. The mutation was verified by DNA sequencing. The protein production and purification of these mutants were done as for the truncated forms described above.

CD spectroscopy

Steady-state CD spectra were measured in the far-UV light (180–260 nm) using a CHIRASCAN spectrometer (Applied Photophysics). Spectra were collected in a 60 μL quartz cell (Hellma) with a path length of 0.1 mm, at 20°C and a step resolution of 1 nm. The readings were averages of 2 s at each wavelength and the recorded milli-degree values were averages of three determinations for each sample. CD spectroscopy of H_{1-47}, H_{1-54}, H_{1-67}, H_{1-71}, H_{1-78}, H_{1-91}, and H_{47-105} (2.0 mg/mL), respectively, was performed in a buffer of 50 mM Tris/HCl (pH 7.5), 250 mM NaCl, and 1 mM DTT. The spectrum for the buffer was subtracted from the spectrum of the protein. CD values were converted to mean residue molar ellipticity (Θ) in units of degree cm^2 $dmol^{-1}$ using the software *Chirascan* version 1.2 (Applied Photophysics). This baseline-corrected spectrum was used as input for computer methods to obtain predictions of secondary structure. To analyze the CD spectrum, the following algorithms were used: VARSLC (21), SELCON3 (22), CONTINLL (23), and K2D (24) (all methods as incorporated into the program Dicroprot (25) and NeuralNet (26)).

Cross-link formation of the truncated forms

The subunit H mutants A19C, A26C, A35C, and A37C, respectively, were supplemented with 10 μM of $CuCl_2$ as a zero length cross-linker for 20 min on a sample rotator at 4°C. The reaction was stopped by addition of 1 mM EDTA. Samples were dissolved in DTT-free dissociation buffer and applied to an SDS-polyacrylamide gel.

NMR data collection and processing

For the production of uniformly labeled (^{15}N and $^{15}N/^{13}C$) H_{1-47}, the expressing bacteria were grown in M9 minimal medium containing $^{15}NH_4Cl$ or $^{15}NH_4Cl/^{13}C$ glucose. The NMR sample was prepared in 90% H_2O/10% D_2O containing 25 mM NaH_2PO_4/Na_2HPO_4/ (pH 6.5) and 0.1% NaN_3. NMR experiments were performed at 10°C and 15°C on a Bruker Avance 600 MHz spectrometer as specified for individual experiments. The experiments recorded using the ^{15}N-labeled sample were 2D ^{15}N-HSQC and 3D ^{15}N-NOESY-HSQC (mixing time: 200 ms). HNCO, HNCACB, CBCA(CO)NH, HCCCONH, and 3D ^{13}C-NOESY-HSQC (mixing time: 200 ms) (27) were collected at 15°C using the $^{15}N/^{13}C$-labeled sample. ^1H chemical shifts were referenced relative to DSS. The chemical shifts of ^{13}C and ^{15}N nuclei were referenced indirectly via ^1H chemical shifts. All NMR spectra were processed using either nmrPipe/nmrDraw (28) or TopSpin (Bruker BioSpin). Spectrum analysis was performed using CARA (www.nmr.ch) and SPARKY (29).

Collection of structural constraints and structure calculations

The structure calculations were performed starting from Met_{10} at the N-terminus located after Pro_9. Distance constraints collection and structure reconstruction were performed using CYANA 3.0 (30,31) with NOEs obtained from 3D ^{15}N-edited NOESY-HSQC, leading to 468 meaningful NOE distance restraints. Dihedral angle restraints were calculated from

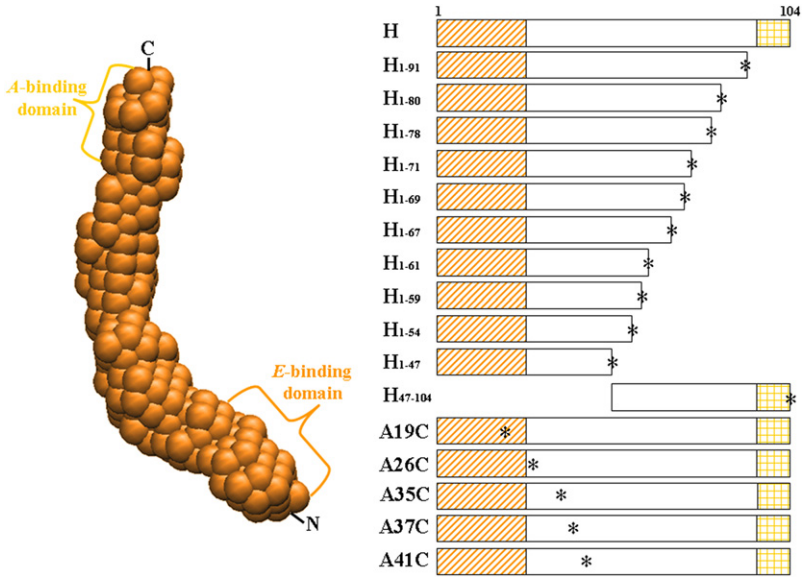

FIGURE 1 Low-resolution structure of subunit H of *M. jannaschii* derived from solution SAXS data (17), with the indicated N- and C-terminal domain binding to subunit E (6) and A (17), respectively. On the right side the constructs of the H subunit used in this study are illustrated. The cysteine residues at the very end of the truncated proteins, as well as the cysteines introduced in the alanine positions (A19C, A26C, A35C, A37C, and A41C) of the subunit H mutants are marked by *. The hatched (*orange*) and squared (*yellow*) regions represent the domains of subunit H interacting with the A_1A_O ATP synthase subunits E and A, respectively.

Cα and Cβ chemical shifts by TALOS (32). Secondary structure was predicted from the chemical-shift index and NOE patterns. Ten calculated conformers with the lowest penalty scores were selected to represent the 3D structure of the monomeric $H_{1\text{-}47}$ and visualized by MOLMOL (33).

^{15}N Relaxation measurements

The ^{1}H-^{15}N steady-state NOE, ^{15}N longitudinal R_1, and transverse R_2 relaxation rates were measured at 10°C using ^{15}N-labeled samples at concentrations of 0.125 mM and 3.0 mM according to the experimental schemes of Palmer et al. (34). ^{15}N decoupling during acquisition was achieved using a GARP-4 pulse sequence (35,36). For R_1, the relaxation delays of 5, 40, 80, 130, 210, 330, 470, 630, 800, and 1000 ms, with duplicated points at 40 ms and 130 ms for error estimations, were recorded. For R_2, data were acquired with delays of 14.4, 28.8, 43.2, 57.6, 72.0, 86.4, 100.8, 115.2, 129.6, 144.0, and 158.4 ms, with duplicated points at 43.2 ms and 72.0 ms. The delay between ^{15}N 180° pulses in the Carr-Purcell-Meiboom-Gill pulse train was set to 0.9 ms. ^{1}H-^{15}N steady-state NOEs were estimated using two datasets collected with and without initial proton saturation for a period of 3 s and interscan delay of 2 s. The relaxation data were interpreted using the programs Modelfree (37) and Fast ModelFree (38).

Diffusion coefficient measurements

The translational diffusion rates were measured by monitoring 1D ^{1}H signal decay due to molecular diffusion in the z-direction of the sample using PFGs (39,40) at variable concentrations of $H_{1\text{-}47}$, $H_{1\text{-}61}$, $H_{1\text{-}69}$, and $H_{1\text{-}80}$, respectively. In each experiment the PFG strength was linearly incremented from 2 to 95 G/cm, with a translational diffusion delay of 200 ms and total encoding and decoding gradient durations of 5 ms. The diffusion rates were estimated using TopSpin (Bruker BioSpin).

RESULTS

Production, purification, and spectroscopic characterization of subunit H

The dimeric subunit H has a boomerang-shape with a ~60 Å long N-terminal arm and a 120 Å long C-terminal tail (Fig. 1) (17). The N-terminal region (residues 1–24) forms the binding epitope for the N-terminal binding of subunit E, as observed in NMR titration experiments (6), whereby the C-terminal amino acids 99–104 are involved in assembly of subunits A and H, as demonstrated by intrinsic fluorescence spectroscopy (14). CD spectroscopy revealed that the protein is 80% α-helical and at least partially in a coiled-coil arrangement, as reflected by the $\Theta_{222}/\Theta_{208}$ ratio of 0.96 (17). The truncated forms $H_{1\text{-}47}$, $H_{1\text{-}54}$, $H_{1\text{-}59}$, $H_{1\text{-}61}$, $H_{1\text{-}67}$, $H_{1\text{-}69}$, $H_{1\text{-}71}$, $H_{1\text{-}78}$, $H_{1\text{-}80}$, $H_{1\text{-}91}$, and $H_{47\text{-}105}$, respectively, were selected in this study (Fig. 1) to explore differences in the structural traits of the various proteins. All 11 recombinant proteins could be isolated in high amounts and in high purity (Fig. 2). Because the mutant proteins comprise truncations at either the N- or C-terminus, the CD spectra were expected to provide evidence for regions of greater helical content, or the nature of helical interactions. CD spectra of the truncated mutants showed large negative ellipticities at Θ_{222} and Θ_{208}, indicative of significant α-helical content in the proteins (Fig. 3, *A* and *B*). Removal of the 14 C-terminal residues of subunit H to produce $H_{1\text{-}91}$ resulted in a 14% and 15% decrease in mean residue ellipticity at 208 and 222 nm, respectively, suggesting a significant decrease in the fraction of

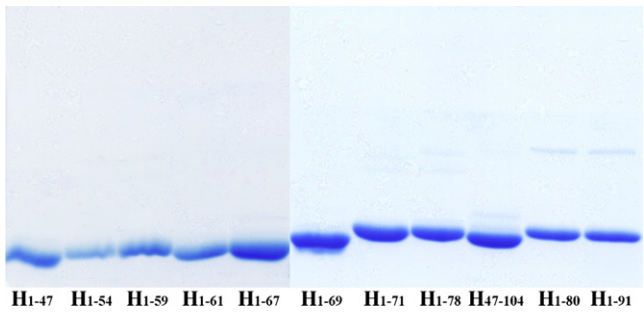

FIGURE 2 SDS polyacrylamide gel (17% total acrylamide and 0.4% cross-linked acrylamide) of the truncated forms $H_{1\text{-}47}$, $H_{1\text{-}54}$, $H_{1\text{-}59}$, $H_{1\text{-}61}$, $H_{1\text{-}67}$, $H_{1\text{-}69}$, $H_{1\text{-}71}$, $H_{1\text{-}78}$, $H_{1\text{-}80}$, $H_{1\text{-}91}$ and $H_{47\text{-}105}$ of the H subunit in the presence of 1 mM DTT.

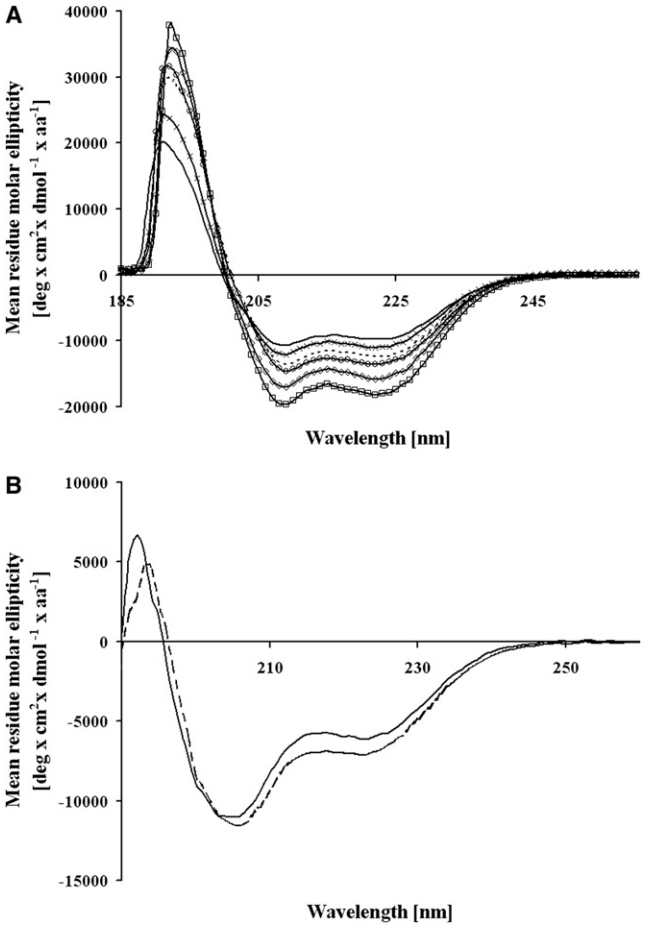

FIGURE 3 (*A*) Far-UV CD spectrum of subunit H subunit (□) and the truncated $H_{1\text{-}67}$ (—), $H_{1\text{-}71}$ (×), $H_{1\text{-}78}$ (- -), $H_{1\text{-}91}$ (◇), and $H_{47\text{-}105}$ (○) proteins, respectively. (*B*) CD spectra of the proteins $H_{1\text{-}47}$ (—) and $H_{1\text{-}54}$ (- -) in 50 mM Tris/HCl (pH 7.5), 250 mM NaCl, and 1 mM DTT at 20°C.

residues in helical conformation. Further removal of 26, 33, and 37 residues from subunit H to obtain $H_{1\text{-}78}$, $H_{1\text{-}71}$, and $H_{1\text{-}67}$ resulted in less negative Θ_{208} and Θ_{222} values, suggesting that removal of the C-terminal residues caused a loss of helical structure in a considerable portion of the C-terminal region. The ratio of the magnitudes of the 222 nm and 208 nm minima ($\Theta_{222}/\Theta_{208}$) for H, $H_{1\text{-}67}$ (61% α-helical), $H_{1\text{-}71}$ (63% α-helical), $H_{1\text{-}78}$ (67% α-helical), and $H_{1\text{-}91}$ (73% α-helical) were 0.96, 0.95, 0.93, 0.92, and 0.91, respectively. By comparison, the CD spectrum of the N-terminal truncated form (46 residues) of $H_{47\text{-}105}$ (69% α-helical) had Θ_{208} and Θ_{222} values higher than the C-terminal truncated constructs $H_{1\text{-}67}$, $H_{1\text{-}71}$, and $H_{1\text{-}78}$ (Fig. 3 *A*). In contrast, a decrease in mean residue ellipticity at Θ_{222} could be observed when the truncated proteins $H_{1\text{-}54}$ and $H_{1\text{-}47}$ (56% α-helical) were analyzed, signifying that these two constructs are less α-helical (Fig. 3 *B*). The observation that $H_{1\text{-}54}$ and $H_{1\text{-}47}$ had a $\Theta_{222}/\Theta_{208}$ ratio of 0.66 and 0.6, respectively, and a blue-shifted minimum compared to the other truncated proteins described above, indicates that this region may not be forming a coiled-coil structure.

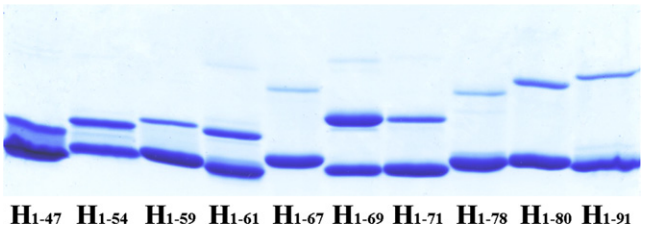

FIGURE 4 Nonreducing SDS-PAGE of $H_{1\text{-}47}$, $H_{1\text{-}54}$, $H_{1\text{-}59}$, $H_{1\text{-}61}$, $H_{1\text{-}67}$, $H_{1\text{-}69}$, $H_{1\text{-}71}$, $H_{1\text{-}78}$, $H_{1\text{-}80}$, and $H_{1\text{-}91}$, demonstrating the disulfide-linked homodimer formation of these constructs.

Disulfide formation within the truncated mutant proteins

Dimer formation was systematically studied by introducing cysteine residues at the very C-terminal end of each of the 11 truncated proteins (Fig. 1). As demonstrated in Fig. 4, the recombinant proteins $H_{1\text{-}54}$, $H_{1\text{-}61}$, $H_{1\text{-}69}$, and $H_{1\text{-}80}$ formed strong dimers in the absence of any oxidizing reagent, with a slightly lower production found for the truncated mutants $H_{1\text{-}47}$, $H_{1\text{-}59}$, $H_{1\text{-}71}$, and $H_{1\text{-}91}$. By contrast, no significant disulfide products were detected for the polypeptides $H_{1\text{-}67}$ and $H_{1\text{-}78}$. This behavior was consistently observed in all repeated experiments.

Solution structure of the N-terminal domain $H_{1\text{-}47}$

Recently, the very N-terminus (residues 1–24) of this truncated protein was shown to form a binding epitope for subunit E (6). To gain deeper insight into the N-terminal segment, we analyzed $H_{1\text{-}47}$ by NMR spectroscopy. The combined carbon (Δ13Cα–Δ13Cβ) secondary shifts of $H_{1\text{-}47}$ (Fig. 5) show a continuous stretch of positive shifts (1.85 ppm) for residues 15–42, indicating a continuous helical structure in this region, with the middle region (residues 15–42) exhibiting markedly higher helical propensity. The 3D structure of subunit $H_{1\text{-}47}$ was calculated based on a total of 468 NOE-derived distance constraints (133 intraresidual, 180 sequential, and 155 medium range), with no unequivocally assigned intermonomeric NOEs. A plot of the NOE connectivities is shown in Fig. S2 of the Supporting Material. Fig. 6 *A* shows 10 lowest-energy conformers of $H_{1\text{-}47}$ superimposed using backbone atoms of residues 15–42 with the structure reconstruction statistics provided in Table 1. Analysis of the

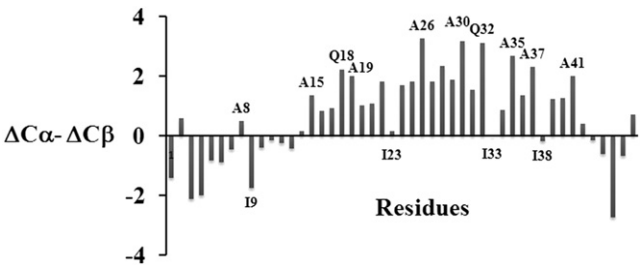

FIGURE 5 Secondary chemical shifts ($\Delta^{13}C\alpha$-$\Delta^{13}C\beta$) of $H_{1\text{-}47}$ in 25 mM phosphate buffer, pH 6.5, at 15°C.

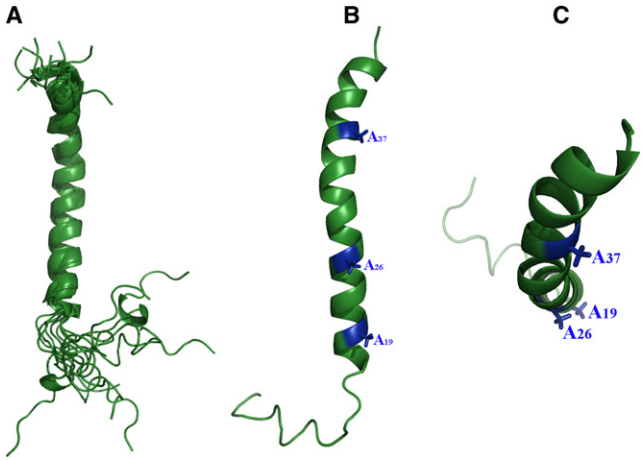

FIGURE 6 Ribbon diagram of the NMR solution structure of $H_{1\text{-}47}$. (*A*) Best-fit superimposition of the 10 lowest-energy NMR structures. Side (*B*) and top (*C*) views of the average structure of $H_{1\text{-}47}$ illustrating the relative positions of alanine residues 19, 26, and 37 inside the α-helix, which are marked in blue.

Ramachandran plots shows that 81.5% residues are in the most favored regions, and 18.5% are in the additionally allowed regions. The regular α-helical conformation was detected for residues A_{15}–K_{42}, with a small kink in the center of the molecule. In the solution structure, $H_{1\text{-}47}$ has a total length of ~60 Å, including the α-helical structure of 43 Å in length.

Dimerization interactions in subunit H mutants

The solution structure of $H_{1\text{-}47}$ reveals a strip of hydrophobic alanine residues made by the residues Ala^{19}, Ala^{26}, and Ala^{37}, with a slight twist toward each other (Fig. 7 *A*). A helical wheel plot of $H_{1\text{-}47}$ shows the close proximity of these alanine residues (Fig. S2). To analyze the proximity of alanine residue of the first and second α-helices of the dimeric H subunit (17), Ala^{19}, Ala^{26}, and Ala^{37}, respectively, were replaced by a cysteine residue, generating the mutants A19C, A26C, and A37C of the entire subunit H. When the mutants were incubated in the absence of an oxidizing reagent, a small amount of dimer formation was observed for mutant A19C, which was decreased in the case of the mutant A26C–A37C (Fig. 7 *B*). Cross-link formation in the presence of $CuCl_2$ (10 μM) is shown in Fig. 8 *B* (lanes 5–8). In the case of mutant A19C, ~50% of the protein formed a dimer when the protein was supplemented with the oxidizing agent. By comparison, the amount of cross-link products was decreased when the mutant protein A26C or A37C was used. In contrast, when the alanine residue 35, located at the opposite site of Ala^{37} (Fig. 7 *A*), was exchanged by a cysteine residue, no disulfide formation could be detected under the conditions used (Fig. 7 *B*, lanes 4 and 8).

TABLE 1 Statistics for the 10 final structural models of $H_{1\text{-}47}$

Total number of NMR restraints	526
Intraresidual ($\|i - j\| = 0$)	133
Sequential ($\|i - j\| = 1$)	180
Short-range ($\|i - j\| \leq 1$)	313
Medium-range ($2 \leq \|i - j\| \leq 5$)	155
Long-range ($\|i - j\| > 5$)	0
Dihedral angle constraints	58
Total number of restraint violations > 0.3 Å	0
Ramachandran plot statistics (%)	
Residues in most favored regions	81.5
Residues in additionally allowed regions	18.5
Residues in generously allowed regions	0
Residues in disallowed regions	0
Structural precision for well-ordered region	
RMSD backbone (residues 15–42):	0.95 Å
RMSD backbone (residues 15–33):	0.68 Å
RMSD backbone (residues 33–42):	0.61 Å

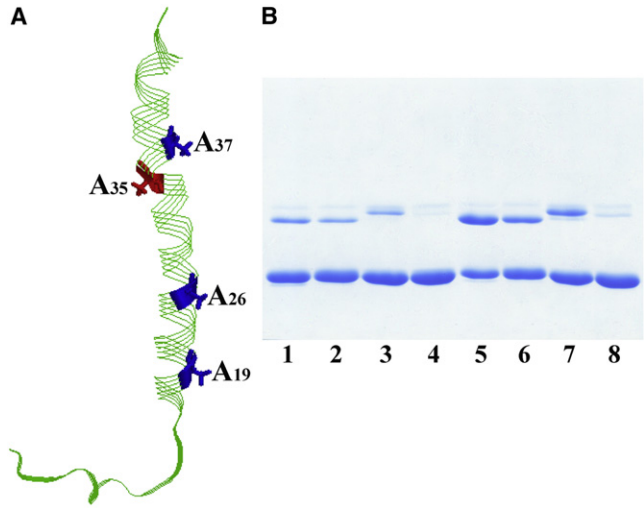

FIGURE 7 (*A*) Solution structure of $H_{1\text{-}47}$ with the alanine residues substituted to cysteine (A19C, A26C, A35C, and A37C). The positions of alanine 19, 26, and 37 are labeled in blue, and alanine 35 is marked in red. (*B*) Cross-linking of the subunit H mutants A19C (lanes 1 and 5), A26C (lanes 2 and 6), A37C (lanes 3 and 7), and A35C (lanes 4 and 8), respectively, in the absence (lanes 1–4) or presence (lanes 5–8) of 10 μM $CuCl_2$. In the latter case, the mutant proteins were incubated with 10 μM $CuCl_2$ for 30 min at 4°C. The reaction was stopped by the addition of 1 mM EDTA. The samples were applied to a 17% total acrylamide and 0.4% cross-linked acrylamide gel.

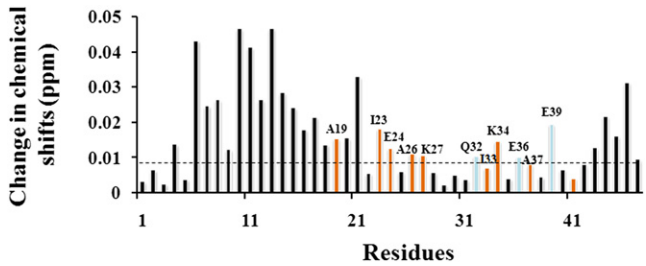

FIGURE 8 Combined amide (^1H) and nitrogen (^{15}N) chemical-shift changes $([(\Delta^1H_N)^2 + (\Delta^{15}N_{ppm}/6.51)^2]^{0.5})$ for $H_{1\text{-}47}$ at concentrations between 3 mM and 0.125 mM. Orange-colored bars represent the residues forming the dimeric interface of $H_{1\text{-}47}$. Charged residues exhibiting large shifts, which are not directly situated at the dimeric interface, are marked in cyan.

Translational diffusion rates

The diffusion coefficients of H_{1-47}, H_{1-61}, H_{1-69}, and H_{1-80} (Fig. S3, *A–D*) were measured as a function of protein concentration. In all cases, the decrease in the experimentally determined diffusion rates with the increasing concentration suggests dimer formation, assuming that the exchange between monomers and dimers is fast on the diffusion timescale. The corresponding dimer dissociation constant for H_{1-47} was estimated by direct fit of the translation diffusion rates as a function of concentration to be 1.5 mM. By comparison, the longer constructs H_{1-61}, H_{1-69}, and H_{1-80} showed a stronger tendency toward dimer formation.

Concentration dependence of ^{1}H, ^{15}N chemical shifts, and ^{15}N relaxation parameters for H_{1-47}

^{1}H and ^{15}N chemical-shift perturbations were monitored in a series of ^{1}H -^{15}N HSQC spectra as a function of the H_{1-47} concentration, which ranged from 0.125 mM up to 3 mM. The variation of the cumulative ^{1}H and ^{15}N shifts at the highest and lowest studied concentrations is shown in Fig. 8. The largest shifts were observed for the continuous N-terminal stretch of residues comprising Met^{6} to Ala^{19}, where structural consolidation upon dimer formation was observed by means of ^{15}N relaxation data. In addition, other important residues, including Ala^{19}, Ile^{23}, Glu^{24}, Ala^{26}, Lys^{27}, Gln^{32}, Ile^{33}, Lys^{34}, Glu^{36}, Ala^{37}, and Glu^{39}, were affected by the formation of dimer.

^{15}N R_1 and R_2 relaxation rates and ^{1}H-^{15}N NOE were measured to obtain a direct estimate of backbone mobility in the monomeric and dimeric forms of H_{1-47}. Generalized order parameters (S^2), internal correlation times (τ_e), and conformational exchange-induced line-broadening (R_{ex}) were calculated using the Lipari and Szabo model-free approach (41,42). S^2 order parameters reflect the spatial restriction of ^{1}H-^{15}N bonds on a timescale of picoseconds to nanoseconds, and range from zero for unconstrained motion to one for completely rigid proteins. Fig. 9 shows the obtained ^{15}N R_1 and R_2 relaxation rates and ^{1}H-^{15}N NOE, as well as the generalized order parameters obtained in the Lipari-Szabo model-free analysis. The corresponding model-free statistics are listed in Tables S1 and S2. The isotropic model for the global rotational diffusion was used. Both the isotropic and axially symmetric anisotropic models provided adequate fitting of the experimental relaxation rates. Because of the almost parallel arrangement of the H-N vectors in two adjacent helices, even a high degree of anisotropy did not significantly affect the obtained order parameters. This fact, as well as the presence of a large portion of the amino acids in poorly structured regions, dictated our choice of the isotropic model as the simplest one to adequately describe the experimental data. With the exception of the terminal residues, the S^2 values for H_{1-47} at high and low concentrations are rather uniform, ranging between 0.66 and 0.85 (Fig. 9 *D*). Their magnitude is characteristic of well-folded proteins, demonstrating that fast internal motions are limited for residues 15–42. The τ_e values are in the picosecond range, as is typically found in well-folded proteins. Almost quantitative doubling of the rotational correlation time from 16 ns to 25 ns for the protein between high and low concentrations unequivocally establishes the dimerization process. The latter is accompanied by structural consolidation at region 4–21, as evidenced by the increase in the corresponding order parameters.

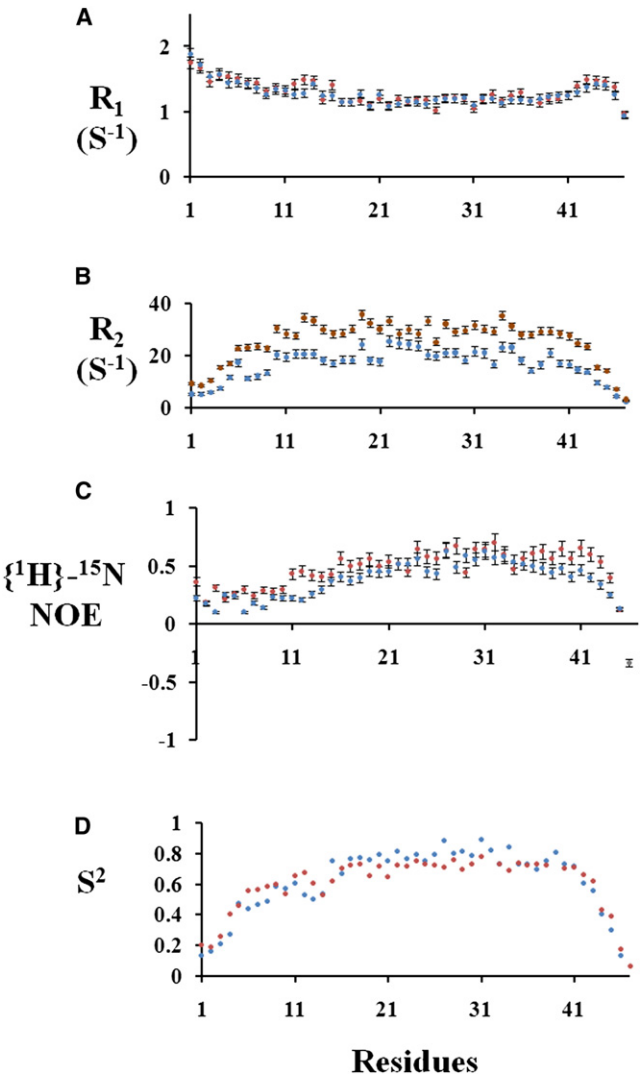

FIGURE 9 (*A*) ^{15}N R_1, (*B*) R_2 relaxation rates, (*C*) $\{^{1}H\}$-^{15}N heteronuclear NOEs for the H_{1-47} at 10°C, and (*D*) Lipari-Szabo order parameter S^2 versus residue number at 3 mM (*brown*) and 0.125 mM (*blue*) concentration of H_{1-47}.

DISCUSSION

Electron microscopy and solution SAXS data reveal a height of the A_3B_3 headpiece and the central stalk of 180 Å. The boomerang-shaped subunit H, which consists of two arms 120 Å and ~60 Å in length (17), extends this distance and

links subunit E with the nucleotide-binding subunit A (6,17). Subunit H is shown to be α-helical (80%) (17). Understanding how the H subunit dimer fulfills its function will require detailed knowledge of its structure. In the work presented here, we studied the domain features of subunit H by using a series of deletions and disulfide formations between introduced cysteines. These results provide a clearer picture of the H subunit architecture and establish for the first time, to our knowledge, that this peripheral stalk is divided into at least two domains. First, the C-terminal part of H, which consists of residues 54–104, is highly α-helical, and the two α-helices in this domain are arranged mostly in a coiled-coil fashion. This is reflected by the high $\Theta_{222}/\Theta_{208}$ ratio of the N-terminal deleted version of subunit H, $H_{47\text{-}105}$, which is higher compared to the C-terminal truncated constructs $H_{1\text{-}67}$, $H_{1\text{-}71}$, and $H_{1\text{-}78}$. It is also in line with the reduced α-helical content of $H_{1\text{-}91}$, $H_{1\text{-}78}$, $H_{1\text{-}71}$, and $H_{1\text{-}67}$, respectively, which corresponds with the deletion size of the C-terminal segement. The existence of subunit H as a pair of parallel helices with a coiled-coil arrangement in region 54–104 is also supported by data showing that cysteine mutants introduced at positions 54, 61, 69, and 80 of the truncated proteins had a strong tendency to form disulfides, whereas a weaker tendency was exhibited at positions 59, 71, and 91, and no significant cross-link was detected at cysteine positions 67 and 78, respectively. This periodicity is consistent with that of a coiled-coil formation, and is supported by the observation that an extensive disulfide bond between the two cysteines at positions 69 and 69′ of the first and second helices was generated, whereas a lower dimer product and only traces of a homodimer were seen for the cysteines at positions 67 and 71, respectively. These data indicate that residue 67 is located at the opposite side of the two helices. In contrast, residues 69 and 71 seem to be a part of the helix-helix interface. The slight shift of the cross-linking pattern between amino acids 71 and 80 is reflected by the amino acid sequence $_{71}$AEKILEETEKE$_{81}$, in which polar residues interrupt the periodicity of the alanine and/or isoleucine pattern that is present in the coiled-coil segment (17). Taken together, the results of these mutagenesis studies enable us to assign the amino acids that participate in the interface of the coiled-coil assembly of two α-helices in the C-terminal domain, and to assign the region of residues 71–81 by showing a shift of periodic hydrophobic interaction between adjacent residues of the two helices.

The second structural domain found in these studies is formed by the N-terminal segment (residues 1–54), which shows a smaller amount of α-helix content with an unstructured stretch in the CD data, as confirmed in the NMR solution structure of $H_{1\text{-}47}$ (Fig. 6). Furthermore, the $\Theta_{222}/\Theta_{208}$ values of 0.6 and 0.66 for $H_{1\text{-}47}$ and $H_{1\text{-}54}$, respectively, support the absence of a coiled-coil assembly in the N-terminal domain and simultaneously reflect the higher dissociation constant of $H_{1\text{-}47}$ compared with the constants of the longer constructs $H_{1\text{-}61}$, $H_{1\text{-}69}$, and $H_{1\text{-}80}$ (Fig. S3, *A–D*).

Our assignment of the coiled coil and dimeric region 54–104, and the N-terminal segment 1–47 suggests that the H subunit is divided into at least two structural parts, and provides a first insight into the two functional domains of subunit H, where the N- and C-termini form the binding epitopes for interaction between subunits A and E, respectively. As pointed out above, the CD spectra of the N-terminal truncations reveal that the N-terminal region has no coiled-coil character. The NMR solution structure of $H_{1\text{-}47}$ exhibits an α-helix formed between amino acids 15–42, including a strip of alanine residues ($Ala^{19,26,37}$) with a slight twist to each other. When these alanine residues exchanged to single cysteine mutants, at none of these positions did disulfide bond formation occur to the extent observed for several mutants detected in the coiled-coil segment (e.g., at positions 54, 61, 69, 71, and 80; Fig. 4)). Only in the presence of 10 μM of the oxidizing agent $CuCl_2$ was a strong disulfide bond formation observed for the subunit H mutant A19C, which was weaker in the two mutants A26C and A37C. These results indicate a closer proximity of residues 19 and 19′ of both helices and support the small twist that the three alanine residues (residues 19, 26, and 37) have relative to each other in the α-helical structure (Fig. 8 *A*). By contrast, the absence of any dimeric product of the A35C mutant is in line with the opposite location of this amino acid relative to the alanine strip shown in the structure, and implies that this residue is located outside of the helix-helix assembly. Taken together, the low coiled-coil content seen in the CD spectra and the low dimeric formation indicate that the major part of the two N-terminal segments ($H_{1\text{-}47}$ and $H_{1\text{-}47'}$) may run in a more adjacent arrangement to each other and come closer at the end of $H_{1\text{-}47}$ and $H_{1\text{-}47'}$. This feature is consistent with the disulfide product seen in $H_{1\text{-}47}$, which became stronger in the seven-residue-longer construct $H_{1\text{-}54}$. The structural switch from a more adjacent to a coiled-coil assembly of both helices inside the dimeric H subunit is facilitated by the small kink at residue 33. This kink is characterized by a break in the chemical-shift index pattern for the helix at this position. The kink also reflects part of the bend in the low-resolution solution structure of the boomerang-like shape of subunit H (17) (Fig. 9 *A*). The overall length (61.9 Å) and structure of $H_{1\text{-}47}$ are remarkably similar with the shorter arm of the shape of subunit H as shown in Fig. 9 *B*. The shape volume enables both helices ($H_{1\text{-}47}$ and $H_{1\text{-}47'}$) to fit in.

NMR measurements obtained with $H_{1\text{-}47}$ as a function of concentration (Fig. S3 *A* and Fig. 9) clearly show that $H_{1\text{-}47}$ forms a dimer at concentrations above ~2 mM. The ^{1}H and ^{15}N chemical-shift perturbations indicate that the residues Ala^{19}, Ile^{23}, Glu^{24}, Ala^{26}, Lys^{27}, Ile^{33}, Lys^{34}, and Ala^{37} may be involved in dimer formation. Based on our structural model, the charged residues Gln^{32}, Glu^{36}, and Glu^{39}, which exhibit comparably large shifts, may not be directly situated at the putative dimeric interface; rather, their side-chain pK_a may be affected via proxy charged residues from the other

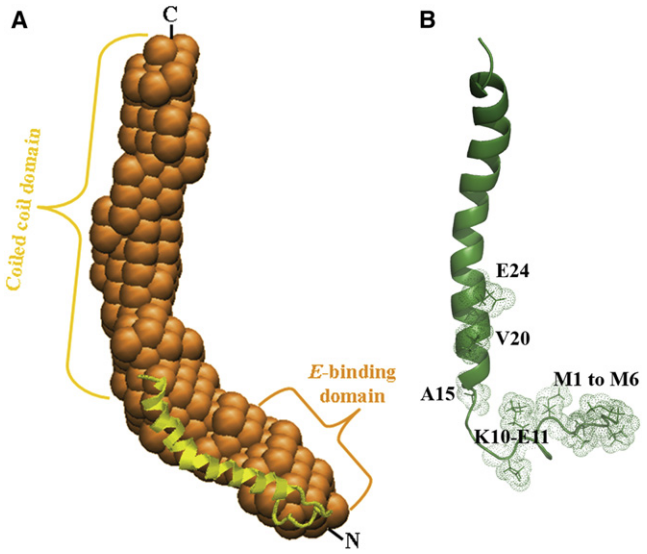

FIGURE 10 (*A*) The H_{1-47} structure is superimposed on the low-resolution structure of the dimeric H subunit derived from solution SAXS data (17). (*B*) The structural model of H_{1-47} enables us to assign the residues involved in subunit E-H formation. Residues M_1–M_6, K_{10}–E_{11}, A_{15}, V_{20}, and E_{24} of H_{1-47} (marked in stick representation, encircled with dotted spheres) were previously shown to interact with the N-terminal tail E_{41-60} of subunit E (6).

monomer. The maximum chemical-shift change was observed for residues 6–21 and 43–47 (Fig. 8). NMR secondary chemical shifts (Fig. 5) as well as ^{15}N relaxation data (Fig. 9, *A–C*) reveal that these regions are less structured as compared to the continuous central α-helix. Some structural consolidation at the N-terminus is seen as the direct consequence of dimerization, as evidenced by the increased order parameters. Therefore, we propose that dimer formation of H_{1-47} may be accompanied by structural consolidation at the flexible regions.

The CD data also suggest that H_{1-47} and H_{1-54} have a smaller amount of α-helix relative to the coiled-coil domain. This is supported by the observation of the unstructured tail of the first 15 amino acids in the presented NMR structure (Fig. 6). Using NMR titration experiments and fluorescence correlation spectroscopy, we recently demonstrated that the N-terminal segment E_{41-60} of subunit E binds specifically to residues Met^{1-6}, Lys^{10}, Glu^{11}, Ala^{15}, Val^{20}, and Glu^{24} of H_{1-47} (Fig. 10 *B*) (6). Since the N-terminus of subunit E is predicted to be α-helical (71%), the E_{41-60} peptide may partially assemble with the N-terminal segment of subunit H via a helix-helix interaction. Like subunit H, the collar subunit E is proposed to be dimeric (15); therefore, both subunits may associate via two heterodimers made up by the N-termini of the two proteins.

SUPPORTING MATERIAL

Three figures and two tables are available at http://www.biophysj.org/biophysj/supplemental/S0006-3495 (09)00858-3.

We thank Ms Ragunathan Priya for assistance in generating the construct H_{1-59}.

S. Gayen received a research scholarship from Nanyang Technological University. This research was supported by A*STAR, Biomedical Research Council (06/1/22/19/467).

REFERENCES

1. Lolkema, J. S., Y. Chaban, and E. J. Boekema. 2003. Subunit composition, structure, and distribution of bacterial V-type ATPase. *J. Bioenerg. Biomembr.* 35:323–336.
2. Murata, T., I. Yamato, and Y. Kakinuma. 2005. Structure and mechanism of vacuolar Na^+-translocating ATPase from *Enterococcus hirae*. *J. Bioenerg. Biomembr.* 37:411–413.
3. Grüber, G., and V. Marshansky. 2008. The relationship of A_1A_O ATPsynthases and V_1V_O ATPases: structural, functional and mechanistical aspects of an energy producer and an energy transducer. *Bioessays.* 30:1096–1109.
4. Coskun, Ü., Y. L. Chaban, A. Lingl, V. Müller, W. Keegstra, et al. 2004. Structure and subunit arrangement of the A-type ATP synthase complex from the archaeon *Methanococcus jannaschii* visualized by electron microscopy. *J. Biol. Chem.* 279:38644–38648.
5. Bernal, R. A., and D. Stock. 2004. Three-dimensional structure of the intact *Thermus thermophilus* H^+-ATPase/synthase by electron microscopy. *Structure.* 12:1789–1798.
6. Gayen, S., A. M. Balakrishna, G. Biuković, W. Yulei, and G. Grüber. 2008. Identification of critical residues of subunit H in its interaction with subunit E of the A-ATP synthase from *Methanocaldococcus jannaschii*. *FEBS J.* 275:1803–1812.
7. Grüber, G., D. I. Svergun, Ü. Coskun, T. Lemker, M. H. J. Koch, et al. 2000. Structural insights into the A_1 ATPase from the archaeon, *Methanosarcina mazei* Gö1. *Biochemistry.* 40:1890–1896.
8. Coskun, Ü., M. Radermacher, V. Müller, T. Ruiz, and G. Grüber. 2004. Three-dimensional organization of the archaeal A_1-ATPase from *Methanosarcina mazei* Gö1. *J. Biol. Chem.* 279:22759–22764.
9. Schäfer, I., M. Rössle, G. Biuković, V. Müller, and G. Grüber. 2006. Structural and functional analysis of the coupling subunit F in solution and topological arrangement of the stalk domains of the methanogenic A_1A_O ATP synthase. *J. Bioenerg. Biomembr.* 38:83–92.
10. Maegawa, W., H. Morita, D. Iyaguchi, M. Yao, N. Watanabe, et al. 2006. Structure of the catalytic nucleotide-binding subunit A of A-type ATP synthase from *Pyrococcus horikoshii* reveals a novel domain related to the peripheral stalk. Acta Crystallogr. *D Biol. Crystallogr.* 62:483–488.
11. Schäfer, I., S. M. Bailer, M. G. Düser, M. Börsch, A. B. Ricardo, et al. 2006. Crystal structure of the archaeal A_1A_O ATP synthase subunit B from *Methanosarcina mazei* Gö1: implications of nucleotide-binding differences in the major A_1A_O subunits A and B. *J. Mol. Biol.* 358:725–740.
12. Iwata, M., H. Imamura, E. Stambouli, C. Ikeda, M. Tamakoshi, et al. 2004. Crystal structure of a central stalk subunit C and reversible association/dissociation of vacuole-type ATPase. *Proc. Natl. Acad. Sci. USA.* 101:59–64.
13. Numoto, N., A. Kita, and K. Mike. 2004. Structure of the C subunit of V-type ATPase from *Thermus themophilus* at 1.85 Å resolution. *Acta Crystallogr. D Biol. Crystallogr.* 60:810–815.
14. Gayen, S., S. Vivekanandan, G. Biuković, G. Grüber, and H. S. Yoon. 2007. The NMR solution structure of subunit F of the methanogenic A_1A_O ATP synthase and its interaction with the nucleotide-binding subunit B. *Biochemistry.* 46:11684–11694.
15. Lokanath, N. K., Y. Matsuura, C. Kuroishi, N. Takahashi, and N. Kunishima. 2006. Dimeric core structure of modular stator subunit E of archaeal H^+-ATPase. *J. Mol. Biol.* 366:933–944.
16. Murata, T., I. Yamato, Y. Kakinuma, A. G. W. Leslie, and J. E. Walker. 2005. Structure of the rotor of the V-type Na^+-ATPase from *Enterococcus hirae*. *Science.* 308:654–659.

17. Biuković, G., M. Rössle, S. Gayen, Y. Mu, and G. Grüber. 2007. Small-angle X-ray scattering reveals the solution structure of the peripheral stalk subunit H of the A_1A_O ATP synthase from *Methanocaldococcus jannaschii* and its binding to the catalytic A subunit. *Biochemistry*. 46:2070–2078.

18. Grüber, G., J. Godovac-Zimmermann, T. A. Link, Ü. Coskun, V. F. Rizzo, et al. 2002. Expression, purification and characterization of subunit E, an essential subunit of the vacuolar-ATPase. *Biochem. Biophys. Res. Commun*. 298:383–391.

19. Laemmli, U. K. 1970. Cleavage of structural proteins during the assembly of the head of bacteriophage T4. *Nature*. 227:680–685.

20. Ho, S. N., H. D. Hunt, R. M. Horton, J. K. Pullen, and L. R. Pease. 1989. Site directed mutagenesis by overlap extension using polymerase chain reaction. *Gene*. 77:51–59.

21. Manavalan, P., and W. C. Johnson, Jr. 1987. Variable selection method improves the prediction of protein secondary structure from circular dichroism spectra. *Anal. Biochem*. 167:76–85.

22. Sreerama, N., and R. W. Woody. 1993. A self-consistent method for the analysis of protein secondary structure from circular dichroism. *Anal. Biochem*. 209:32–44.

23. Provencher, S. W. 1982. A constrained regularization method of inverting data represented by linear algebraic or integral quations. *Comput. Phys. Commun*. 27:213–227.

24. Andrade, M. A., P. Chacon, J. J. Merelo, and F. Moran. 1993. Evaluation of secondary structure of proteins from UV circular dichroism spectra using an unsupervised learning neural network. *Protein Eng*. 6:383–390.

25. Deléage, G., and C. Geourjon. 1993. An interactive graphic program for calculating the secondary structures content of proteins from circular dichroism spectrum. *Comput. Appl. Biosci*. 9:197–199.

26. Böhm, G. 1992. Quantitative analysis of protein far UV circular dichroism spectra by neural networks. *Protein Eng*. 5:191–195.

27. Sattler, M., J. Schleucher, and C. Griesinger. 1999. Heteronuclear multidimensional NMR experiments for the structure determination of proteins in proteins employing pulsed field gradients. *Prog. Nucl. Magn. Reson. Spectrosc*. 34:93–158.

28. Delaglio, F., S. Grzesiek, G. W. Vuister, G. Zhu, J. Pfeifer, et al. 1995. NMRPipe: a multidimensional spectral processing system based on UNIX. *J. Biomol. NMR*. 6:277–293.

29. Kneller, D. G., and T. D. Goddard. 1997. SPARKY 3, 105 ed. University of California, San Francisco, CA.

30. Wüthrich, K. 1986. NMR of Proteins and Nuclei Acids. Wiley Interscience, New York.

31. Herrmann, T., P. Güntert, and K. Wüthrich. 2002. Protein NMR structure determination with automated NOE assignment using the new software CANDID and the torsion angle dynamics algorithm DYANA. *J. Mol. Biol*. 319:209–227.

32. Cornilescu, G., F. Delaglio, and A. Bax. 1999. Protein backbone angle restraints from searching a database for chemical shift and sequence homology. *J. Biomol. NMR*. 13:289–302.

33. Koradi, R., M. Billeter, and K. Wüthrich. 1996. MOLMOL: a program for display and analysis of macromolecular structures. *J. Mol. Graph*. 14:51–55.

34. Palmer, A. G., J. Williams, and A. McDermott. 1996. Nuclear magnetic resonance studies of biopolymer dynamics. *J. Phys. Chem*. 100:13293–13310.

35. Shaka, A. J., P. B. Barker, and R. Freeman. 1985. Computer optimized decoupling scheme for wideband applications and low-level operation. *J. Magn. Reson*. 64:547–552.

36. Pervushin, K., G. Wider, and K. Wüthrich. 1997. Deuterium relaxation in a uniformly ^{15}N labelled homeodomain and its DNA complex. *J. Am. Chem. Soc*. 119:3842–3843.

37. Mandel, A. M., M. Akke, and A. G. Palmer. 1995. Backbone dynamics of *Escherichia coli* ribonuclease HI: correlations with structure and function in an active enzyme. *J. Mol. Biol*. 246:144–163.

38. Cole, R., and J. P. Loria. 2003. FAST-Modelfree: a program for rapid automated analysis of solution NMR spin-relaxation data. *J. Biomol. NMR*. 26:203–213.

39. Gibbs, S. J., and C. S. J. Johnson. 1969. A PFG NMR experiment for accurate diffusion and flow studies in the presence of eddy currents. *J. Magn. Reson*. 93:395–402.

40. Wilkins, D. K., S. B. Grimshaw, V. Receveur, C. M. Dobson, J. A. Jones, et al. 1999. Hydrodynamic radii of native and denatured proteins measured by pulse field gradient NMR techniques. *Biochemistry*. 38:16424–16431.

41. Lipari, G., and A. Szabo. 1982. Model-free approach to the interpretation of nuclear magnetic resonance relaxation in macromolecules. 1. Theory and range of validity. *J.J. Am. Chem. Soc*. 104:4546–4559.

42. Jarymowycz, V. A., and M. J. Stone. 2006. Fast time scale dynamics of protein backbones: NMR relaxation methods, applications, and functional consequences. *Chem. Rev*. 106:1624–1671.